Advanced self-assembly control of rod-shaped organic semiconductors

S. Arai*[a]
[a]National Institute for Materials Science, 1-1 Namiki, Tsukuba, Ibaraki, Japan 305-0044
*ARAI.Shunto@nims.go.jp; phone +81-29-860-4331

ABSTRACT

Numerous rod-like organic molecules self-organize into layered structures, as demonstrated in various systems, including smectic liquid crystals, micelles, and lipid bilayers, owing to side-by-side intermolecular interactions. These layered structures are of interest to another class of layered molecular assemblies in the solid state, namely, small-molecule organic semiconductors (OSCs). Many OSCs are composed of various π-electron cores substituted with flexible side chains. Layered-structure formation is important in OSC systems because it enables the production of aligned molecular layers interfaced with gate dielectric layers, which are used to fabricate high-performance organic thin-film transistors (OTFTs). Using these rod-shaped OSCs, we developed a technique for fabricating single-crystal thin films of uniform thickness at the molecular level by introducing a geometric frustration effect between the layers. We also selectively produced crystalline polymorphs with distinct herringbone packing motifs. By producing these layer-controlled films on the trap-minimized surface of gate insulators, we fabricated OTFTs exhibiting sharp on/off switching characteristics approaching the Boltzmann limit. In this paper, we introduce recent techniques for the rational design of organic semiconductors.

Keywords: self-assembly, molecular bilayer, crystal engineering, organic semiconductors, smectic liquid crystals

1. INTRODUCTION

Rod-shaped molecules tend to self-organize into layered molecular assemblies, as observed in lipid bilayers and smectic liquid crystals [1]. Recently, these layered structures have been extensively investigated in different classes of solid-state materials, such as organic semiconductors (OSCs). In OSCs systems, many molecules are composed of π-electron cores (π-cores) substituted by long alkyl chains [2–4]. Alkylation enhances the layered crystalline nature of OSCs owing to the side-by-side intermolecular interactions. This layered crystallinity is a critical requirement for efficient carrier transport within the layer and is suitable for applications in organic thin-film transistors (OTFTs) [5, 6].

Previous studies have demonstrated that layered crystallinity is considerably enhanced using an unsymmetrical alkylation of OSCs, as was demonstrated in benzothieno[3,2-*b*][1]benzothiophene (BTBT) [5, 6], benzothieno[3,2-*b*]naphtho[2,3-*b*]thiophene (BTNT) [7, 8], and benzothieno[6,5-*b*]benzothieno[3,2-*b*]thiophenes (BTBTT) derivatives [9, 10]. The asymmetric OSC molecules basically provide bilayer-type packing, where the molecules separately form π-core and inert alkyl chain layers. Pairs of the unipolarly oriented molecular layers are coupled to form an alternating antiparallel alignment, such that the alkyl chain layers (π-core layers) are in tail-to-tail (head-to-head) contact, being reminiscent of the cell membrane. The separated formation of a 2D semiconductive π-core layer and inert alkyl-chain layers should eventually contribute to the enhancement of the layered crystallinity [8]. Another intriguing aspect is that these materials frequently undergo smectic liquid–crystal phase transitions at elevated temperatures, as observed in phenyl-alkylated BTBT (Ph-BTBT-C$_n$) [11].

This study provides an overview of crystal structure control in layered OSCs and its effect on OTFT performance. First, the stacking control of molecular layers is demonstrated. Second, the polymorphic control of the molecular arrangement within the layers is presented. In these studies, the flexible alkyl chain plays an important role in tuning the crystal structure. Subsequently, the origin of the differences in the carrier transport properties of the polymorphs based on the transfer integral and energy band structure results is discussed. Finally, by combining crystal structure engineering with device optimization, it is demonstrated that sharp on/off switching characteristics of OTFTs can be reproducibly fabricated.

Emerging Liquid Crystal Technologies XIX, edited by Liang-Chy Chien, Nelson V. Tabiryan, Jun Yamamoto, Proc. of SPIE Vol. 12907, 1290705 · © 2024 SPIE
0277-786X · doi: 10.1117/12.3001198

2. RESULTS AND DISCUSSION

2.1 Thickness control of layered molecular crystals

Herein, we focus on *mono*-C_n-BTBT, a simple system in which an alkyl chain is attached to only one side of the BTBT backbone. Its molecular structure is shown in **Figure 1(a)**. A molecule crystallizes into a bilayer-type packing motif when the number of carbon atoms in the alkyl chain $n \geq 4$ [6, 12]. From the direction of the molecular long axis, the π-electron backbone is arranged in a herringbone shape within the layer (**Figure 1(b)**).

Crystalline thin films were prepared from a solution of these molecules using the blade coating method (EXPERIMENTAL SECTION) [13]. The optical microscopy images of the resulting crystals are shown on the left side of **Figure 1(c)**. The different colors of the thin films indicate thickness differences, with regions of common colors showing homogeneous thickness at the molecular level. Cross-Nicol observations and X-ray diffraction confirmed that the regions of homogeneous thickness were single crystals.

Multilayered regions possess inert alkyl chain layers, producing access resistance in top-contact OTFTs [13]. Access resistance reduces the effective carrier mobility of OTFTs in thick films. Therefore, we consider that molecularly thin crystals with homogeneous thickness must be fabricated. In this study, we introduced a structure that was incompatible with the stacking order of molecular films by mixing molecules with different alkyl chain lengths [14], as shown in **Figure 1(d)**. Few molecules with longer chain lengths were introduced to act as protrusions on the surface of the molecular film and inhibit stacking. Such structures, which are incompatible with the long-range order, are associated with geometrical frustration effects, which are also observed in liquid crystals. The thin film produced by introducing the frustration effect is shown on the right side of **Figure 1(c)**. The obtained films were homogeneous at the molecular level with a thickness of less than 5 nm. This thickness coincides with that of a single molecular bilayer of the compounds. The geometrical frustration effect is also applicable to analogs of these OSCs because it is based on a simple mechanism.

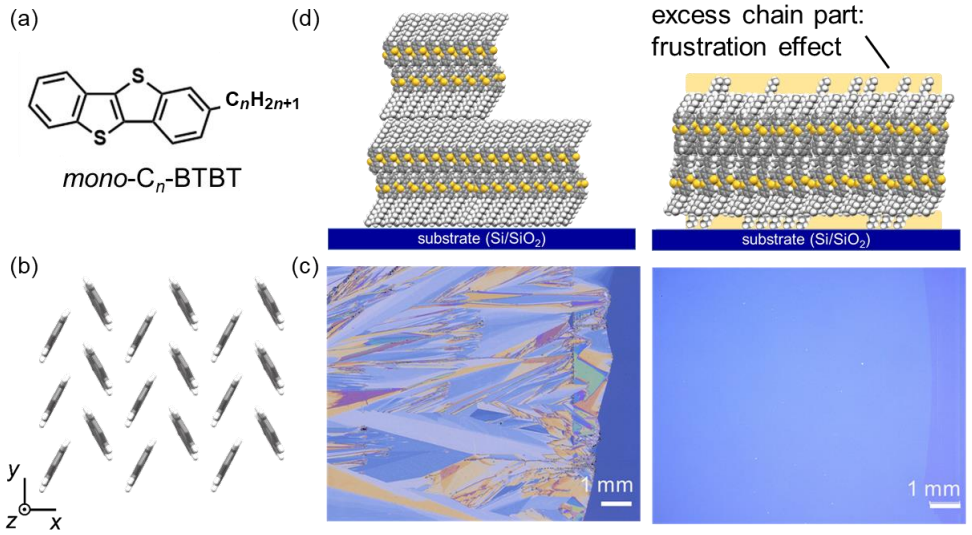

Figure 1. Layer-controlled molecular crystal formation. (a) Chemical structure of *mono*-C_n-BTBT. (b) Molecular packing motif of *mono*-C_n-BTBT within the layer viewed along the molecular long axes. (c) Fabricated thin films of *mono*-C_{10}-BTBT (left) and a mixed crystal of *mono*-C_{10}-BTBT and *mono*-C_{14}-BTBT with a ratio of 9:1 (right). (d) Schematic of bilayer crystals of *mono*-C_n-BTBTs. (left) Normal stacked bilayer crystal and (right) mixed crystal that embraces alkyl chain length disorder.

2.2 Polymorphic control within the layer

In addition to controlling the stacking, two different crystal polymorphs with a common bilayer structure but different intralayer arrangements can be observed [15, 16]. This polymorphism is specific to the layered herringbone (LHB)-type arrangement. The packing structures are shown in **Figure 2**. These are the crystal polymorphs found in *mono*-C_n-BTBT, and their packing motifs show the arrangement of the BTBT cores along the molecular long axis. To indicate the differences in the arrangement of the sulfur atoms, different colors associated with the positions of the alkyl chain (i.e., the closer and farther ones are yellow and orange, respectively) are used. These arrangements show that the middle lane (blue dashed line in **Figure 2 (b) and (c)**) has a similar arrangement, but each molecule in the adjacent lane arrangement (magenta dashed line in **Figure 2 (b) and (c)**) has a flipped arrangement.

These crystalline polymorphs are found for short ($4 \leq n \leq 7$) and long ($8 \leq n$) substituted alkyl chains. Therefore, the packing motifs are called short-chain-type polymorphs (SCPs) and long-chain-type polymorphs (LCPs). Calculations of intermolecular interactions have revealed that a SCP is more stable regarding the arrangement of the π-cores compared with the LCP. The SCP-type arrangement of π-cores is selected for BTBT without substituted alkyl chains. In contrast, LCP packing is advantageous for interactions between neighboring alkyl chains within the layer. Thus, the LCP phase is selected based on the delicate balance of intermolecular interactions as the chain length increases [15, 16]. Moreover, interchain interactions are destabilized by increasing the temperature, leading to a crystal–crystal phase transition from the LCP layer to the SCP layer [16].

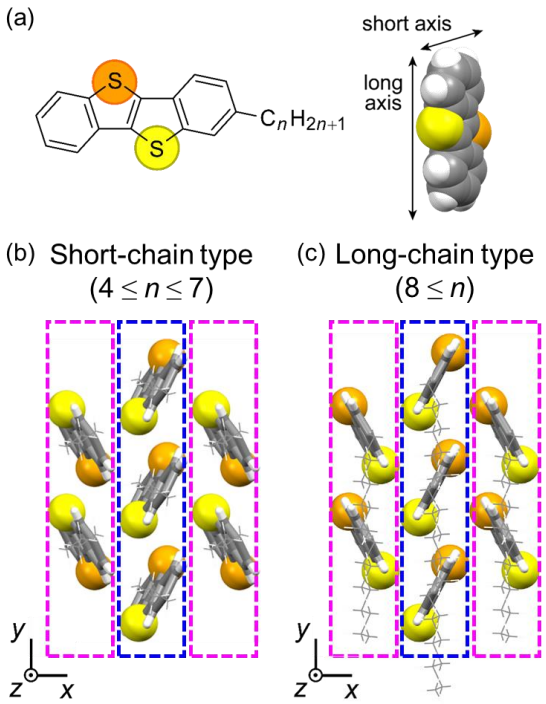

Figure 2. Layered herringbone polymorphism. (a) Schematic of the difference in the coloration of sulfur atoms. (b, c) Distinct glide symmetries in the layered herringbone polymorphs of *mono*-C_n-BTBTs. (b) $n = 4$ (SCP; short-chain polymorph) and (c) $n = 9$ (LCP; long-chain polymorph). The long axes of π-cores align perpendicular to the layer.

2.3 Effect of crystal structure polymorphism on carrier transport performance

To understand the effects of this polymorphism, the charge transport characteristics of *mono*-C_4-BTBT (SCP) and *mono*-C_9-BTBT (LCP) were compared. Single-crystalline thin films of both materials were fabricated and used as active layers in OTFTs [16]. The device mobility of the *mono*-C_4-BTBT TFTs was $\mu_{sat} = 0.20$ cm^2 V^{-1} s^{-1} along the *x* direction and 0.45 cm^2 V^{-1} s^{-1} along the *y* direction. The *x* and *y* directions indicate the crystallographic axes, as shown in **Figure 2 (b,**

c). These values are approximately ten times smaller than those of *mono*-C_9-BTBT TFTs, μ_{sat} = 2.6 and 5.5 $cm^2\ V^{-1}\ s^{-1}$ along the *x* and *y* directions, respectively.

These differences may stem from differences in the intralayer LHB arrangement. Comparing the values of the transfer integrals calculated from the experimentally obtained crystal structures, as shown in **Figure 3(a)**, the transfer integrals in the slipped parallel configuration showed similar values for the SCP and LCP, whereas the values in the *T*-shaped configuration were significantly different. This difference arises from the different molecular orientations of the *T*-shaped contacts between the SCP and LCP. The electronic structures of each crystal were calculated (EXPERIMENTAL SECTION). **Figure 3(b) and (c)** show the corresponding band structures. The effective masses of holes were calculated from the band structures, and the values were 18.4 m_e (*x* direction) and 4.45 m_e (*y* direction) for the SCP, whereas the values were approximately 10 times higher than 1.65 m_e and 1.27 m_e for the LCP, in the *x* and *y* directions, respectively. m_e denotes the masses of the electrons. The results show that the effective mass calculated from the band structure correlates well with the carrier-transport properties of single-crystal OTFTs.

The band structures were affected by the arrangement of π-cores. We also calculated the band structures for differently layered OSCs with a BTBT skeleton showing LCP-type packing motifs. **Figure 4** shows the results of the Ph-BTBT-C_n and *di*-BTBT-C_n systems. Both crystals formed an LCP-type arrangement by introducing long alkyl chain(s), and the band structures were similar to those of the LCP phase of *mono*-C_n-BTBT. Both these materials have been reported to exhibit relatively high mobility, indicating that crystal structure engineering is key for achieving high device mobility.

Finally, we present the performance of OTFTs fabricated by combining crystal structure and device engineering. We previously reported that the sharp on/off switching performance of OTFTs can be realized by fabricating an ultrathin OSC layer on a highly liquid-repellent insulating polymer layer, Cytop [17]. Based on this method, OTFTs were fabricated using OSCs with LCP-type polymorphisms. By mixing and crystallizing molecules with different chain lengths, an ultrathin single-crystal thin film was fabricated using the interlayer frustration effect. Typical TFT characteristics are shown in **Figure 5**. This OTFT can be driven at low voltages below 2 V and shows good carrier transport performance with mobility exceeding 10 $cm^2\ V^{-1}\ s^{-1}$. This shows that understanding and controlling the molecular arrangement is extremely effective for improving the performance of organic devices.

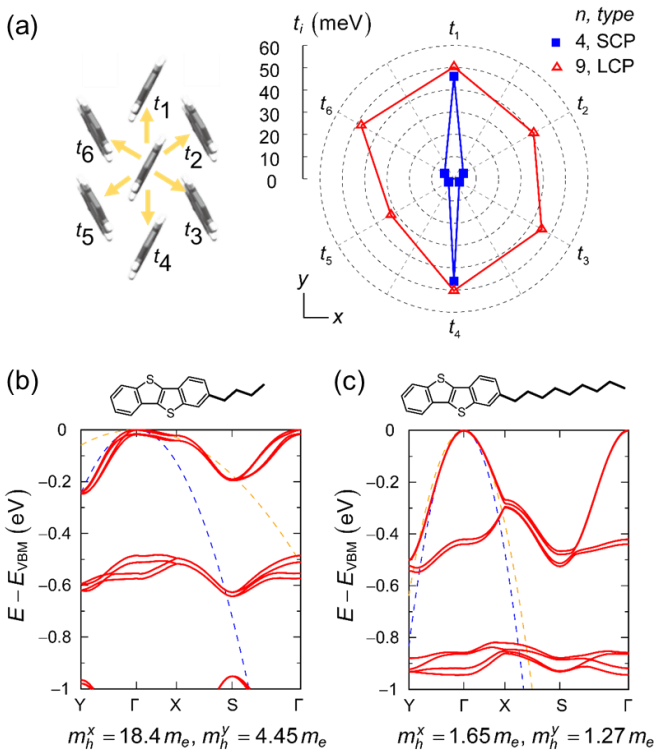

Figure 3. (a) Schematic of the layered herringbone (LHB)-type packing motif. (b) Calculated transfer integrals for *T*-shaped and slipped parallel configurations in LHB packing motifs. (c) Calculated electronic band structures and effective masses of holes along the crystal *a** (m_X*) and *b** (m_Y*) axes. m_e denotes the mass of an electron.

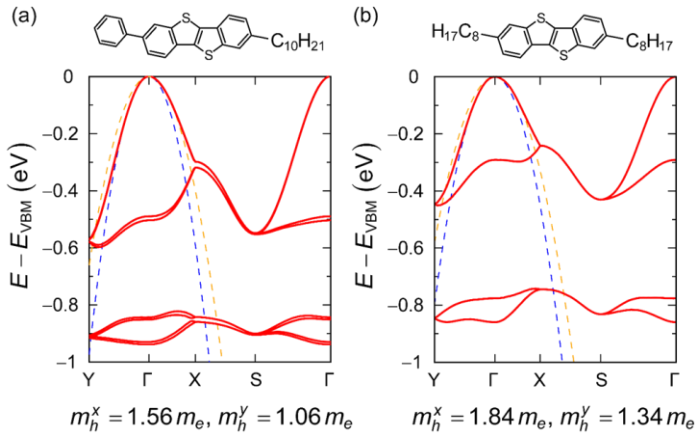

Figure 4. Calculated band structures for (a) Ph-BTBT-C$_n$ and (b) *di*-BTBT-C$_n$.

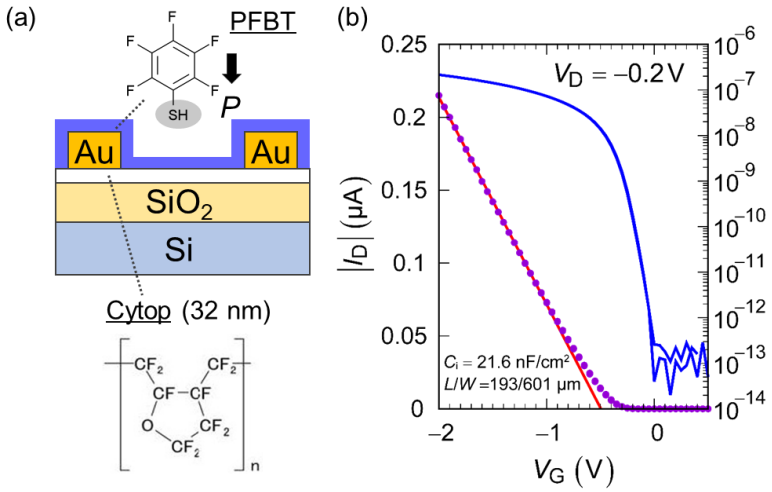

Figure 5. Performance of the fabricated OTFT. (a) Schematic of the cross section of bottom-gate bottom-contact (BGBC)-type TFTs. The surfaces of the source and drain electrodes were modified with pentafluorobenzenethiol (PFBT). (b) Typical device performance of the fabricated OTFT.

3. CONCLUSIONS

In this paper, we provide an overview of the crystal engineering of layered OSCs. By exploiting the tunable nature of substituents such as alkyl chains, we successfully controlled the thickness of the molecular crystal and intralayer packing motifs. We also show that the transfer integral in *T*-shape molecular contacts and the resulting energy band structure are significantly affected by crystal polymorphism. The difference in the effective mass calculated from the band structure correlates well with the carrier-transport properties of single-crystal OTFTs. This indicates that the performance of OTFTs can be improved by polymorphic control of layered OSCs, even if they have the same semiconductor backbone. High-performance OSCs show similar energy band structures associated with the similar symmetry of π-core arrangements. We also found that OTFTs with an extremely steep switching performance could be achieved by fabricating a crystal-structure-engineered OSC layer on the surface of the Cytop insulating layers. We believe that these findings open the possibility for the rational design of layered OSCs for controlling the molecular packing motifs in flexible displays and sensors.

4. EXPERIMENTAL SECTION

4.1 Thin-film fabrication and characterization

Powdered materials were synthesized and purified as previously described. We prepared 0.8 wt% solutions of *mono*-C_n-BTBTs by dissolving the powdered materials in chlorobenzene (FUJIFILM Wako Pure Chemical Corporation, Japan). The solution concentration was sufficiently lower than its saturation concentration. We used a heavily *p*-doped silicon wafer covered with a 100 nm thermally grown silica layer as the substrate for device fabrication. The substrate was cleaned via 3-min sequential sonication in deionized water, acetone, isopropanol, and deionized water. Single-crystalline thin films were produced using a blade coating technique. A thin glass plate coated with Cytop (CTL-809M, AGC Inc., Japan) was used as the coating blade and its motion was controlled using a stepping motor (SHOT-302GS; Sigmakoki Co., Ltd., Japan). Blade coating was performed at a sweep rate of 4−10 μm s^{-1} under ambient conditions.

The fabricated thin films were observed using a digital microscope (VHX-6000, Keyence, Japan). We also used crossed Nicols-polarized optical microscopy to observe the single-crystal domains within the films. The height profile was measured at the rim of the film using atomic force microscopy.

4.2 Preparation and characterization of OTFTs

We prepared a Cytop solution diluted using the solvent (CT-Solv.180; AGC Inc., Japan) at a volume ratio of 1:4 and formed a gate dielectric layer on the silica surface by spin coating at 2000 rpm for 60 s. Subsequently, the Cytop layer was cured at 80 °C for 15 min at 0.02 MPa and 180 °C for 60 min at 0.02 MPa. After drying, source and drain electrodes with 0.5-nm-thick Cr and 25-nm-thick Au were deposited via thermal evaporation on the Cytop surface. The electrode surfaces were then modified by CVT with PFBT (> 95.0%; Tokyo Chemical Industry Co., Ltd., Japan) in a closed container. Thereafter, each OSC solution was coated onto the substrate at room temperature (25 °C). For a proper mobility evaluation, parts of the thin films outside the channel were trimmed using a micromanipulator (Axis-Pro; Systems Engineering Inc., Japan). The conventional two-probe characteristics of the bottom-gate top-contact TFTs were measured using a semiconductor parametric analyzer (E5270A; Agilent Technologies Co. Ltd., USA).

4.3 Theoretical calculations

Intermolecular transfer integrals were also calculated by DFT calculations using the Gaussian 16 program package [18], based on the molecular packing geometries obtained from CSD. We used the PBEPBE/6-311G** level of calculation. The transfer integral t_{AB} between the molecular orbitals $|A\rangle$ and $|B\rangle$ was calculated using the following equation:

$$t_{AB} = \frac{\langle A|F|B\rangle - \frac{1}{2}\left(\langle A|F|A\rangle + \langle B|F|B\rangle\right)S_{AB}}{1 - {S_{AB}}^2},$$

where F is the Fock matrix and S_{AB} is the special overlap integral between the orbitals of the two monomers.

The electronic structures were calculated using a plane-wave basis set and pseudopotentials as implemented in the Quantum Espresso (QE) program [19, 20]. Calculations were performed based on the crystal structures obtained from the CSD. We employed the PBE level of theory with D3BJ dispersion correction [21]. Self-consistent calculations were conducted with cut-off energies of the plane wave basis set and charge densities of 25 and 225 Ry, respectively, and Brillouin-zone integrations of a 3 × 3 × 1 *k*-points mesh. We evaluated the hole effective mass m_h from the curvature of the valence band at the Γ point.

ACKNOWLEDGMENTS

The content of this article is based on the results obtained from fruitful collaborations with many colleagues, including Tatsuo Hasegawa, Toshiki Higashino, Satoru Inoue, Ryusuke Kondo, Reiji Kumai, Mutsuo Tanaka, Jun'ya Tsutsumi, and Seiji Tsuzuki (in alphabetical order). The authors thank all of them for their collaborations and discussions. This study was partially supported by JSPS KAKENHI, Grant No. JP21H05234 and No. JP22H01933; JST PRESTO, Grant No. JPMJPR23N1; and the MEXT Leading Initiative for Excellent Young Researchers Grant No. JPMXS0320220012.

REFERENCES

[1] J. W. Goodby *et al*., "Transmission and Amplification of Information and Properties in Nanostructured Liquid Crystals," *Angew. Chem. Int. Ed*., **47**, 2754-2787 (2008).
[2] J. Mei, Y. Diao, A. L. Appleton, L. Fang, and Z. Bao, "Integrated materials design of organic semiconductors for field-effect transistors," *J. Am. Chem. Soc*. **135**, 6724 (2013).
[3] H. Sirringhaus, "25th anniversary article: Organic field-effect transistors: The path beyond amorphous silicon," *Adv. Mater*. **26**, 1319 (2014).
[4] T. Lei, J.-Y. Wang, and J. Pei, "Roles of flexible chains in organic semiconducting materials," *Chem. Mater*. **26**, 594 (2014).

[5] S. Inoue *et al*., "Effects of Substituted Alkyl Chain Length on Solution-Processable Layered Organic Semiconductor Crystals," *Chem*. *Mater*. **27**, 3809-3812 (2015).
[6] H. Minemawari *et al*., "Enhanced layered herringbone packing due to long alkyl chain substitution in solution-processable organic semiconductors," *Chem*. *Mater*. **29**, 1245 (2017).
[7] S. Inoue *et al*., "Extended and modulated thienothiophenes for thermally durable and solution processable organic semiconductors," *Chem*. *Mater*. **30**, 5050 (2018).
[8] T. Higashino, S. Inoue, Y. Sadamitsu, S. Arai, S. Horiuchi, and T. Hasegawa, "Bilayer-type layered herringbone packing in 3-*n*-octyl-9-phenyl-benzothieno[3,2-*b*]naphtho[2,3-*b*]thiophene," *Chem*. *Lett*. **48**, 453 (2019).
[9] K. He *et al*., "Five-ring-fused asymmetric thienoacenes for high mobility organic thin-film transistors: The influence of the position of the S atom in the terminal thiophene ring," *J*. *Mater*. *Chem*. *C* **7**, 3656 (2019).
[10] T. Higashino *et al*., "Architecting layered crystalline organic semiconductors based on unsymmetric π-extended thienoacenes," *Chem*. *Mater*. **33**, 7379 (2021).
[11] H. Iino, T. Usui and J.-I. Hanna, "Liquid crystals for organic thin-film transistors," *Nat*. *Commun*. **6**, 6828 (2015).
[12] G. Gbabode *et al*., "X-ray structural investigation of nonsymmetrically and symmetrically alkylated [1]benzothieno[3, 2-*b*]benzothiophene derivatives in bulk and thin films," *ACS Appl*. *Mater*. *Interf*. **6**, 13413 (2014).
[13] T. Hamai, S. Arai, H. Minemawari, S. Inoue, R. Kumai, and T. Hasegawa, "Tunneling and origin of large access resistance in layered-crystal organic transistors," *Phys*. *Rev*. *Appl*. **8**, 054011 (2017).
[14] S. Arai, S. Inoue, T. Hamai, R. Kumai, and T. Hasegawa, "Semiconductive single molecular bilayers realized using geometrical frustration," *Adv*. *Mater*. **30**, 1707256 (2018).
[15] S. Arai, K. Morita, J. Tsutsumi, S. Inoue, M. Tanaka, T. Hasegawa, "Layered-herringbone polymorphs and alkylchain ordering in molecular bilayer organic semiconductors," *Adv*. *Funct*. *Mater*. **30**, 1906406 (2020).
[16] S. Arai *et al*., "Temperature-induced transformation between layered herringbone polymorphs in molecular bilayer organic semiconductors," *Phys*. *Rev*. *Mater*. **7**, 025602 (2023).
[17] G. Kitahara *et al*., "Meniscus-controlled printing of single-crystal interfaces showing extremely sharp switching transistor operation," *Sci*. *Adv*. **6**, eabc8847 (2020).
[18] M. J. Frisch *et al*., Gaussian 16 (Wallingford, Connecticut, 2016).
[19] P. Giannozzi *et al*., "QUANTUM ESPRESSO: A modular and opensource software project for quantum simulations of materials," *J*. *Phys*.: *Condens*. *Matter* **21**, 395502 (2009).
[20] P. Giannozzi *et al*., "Advanced capabilities for materials modelling with QUANTUM ESPRESSO," *J*. *Phys*.: *Condens*. *Matter* **29**, 465901 (2017).
[21] S. Grimme, S. Ehrlich, and L. Goerigk, "Effect of the damping function in dispersion corrected density functional theory," *J*. *Comput*. *Chem*., **32**, 1456-1465 (2011).